Molecular Dynamics Studies of Hydrofluorocarbons in Faujasite-type Zeolites: Modeling Guest-Induced Cation Migration in Dry Zeolites

Eugenio Jaramillo,[†] Clare P. Grey,[‡] and Scott M. Auerbach*,[†,§]

Departments of Chemistry and Chemical Engineering, University of Massachusetts, Amherst, Massachusetts 01003, and Department of Chemistry, SUNY Stony Brook, Stony Brook, New York 11794

We have developed and applied a new force field for simultaneously modeling the dynamics of hydrofluorocarbons (HFCs) and exchangeable Na cations in faujasite-type zeolites. Our aim is to account for (i) the zeolite's capacity of separating HFC isomers, (ii) the experimentally observed unusual cation migration in Na−Y from the β-cages into the supercages upon the adsorption of HFCs, and (iii) the abnormal trans/gauche ratio in these systems. Energy minimizations and molecular dynamics simulations performed with this force field give excellent agreement with experimental data on heats of adsorption, guest−host distances, infrared spectra, and conformer ratios for different coverages of HFC-134 ($CF_2H−CF_2H$) and HFC-134a ($CH_2F−CF_3$) in Na−X (Si:Al = 1.2) and Na−Y (Si:Al = 2.4). The force field also accounts partially for the observed cation migration at intermediate loadings and fully at high loadings. The extent of migration is found to be influenced by the competition among Na−O, Na−F, and Na−Na interactions. The Na−O interaction disfavors migration because Na(I′) sites are found to be energetically more favorable than Na(III′) sites; the Na−F attraction obviously favors migration; and surprisingly, the Na−Na repulsion also favors migration because moving Na cations into supercages leads to better cation dispersion. This migration occurs in a two-step mechanism that involves first a concerted two-cation jump, $S_{I}{}' \rightarrow S_{II}{}'/S_{II} \rightarrow (S_{III}$ or $S_{III}{}')$, followed by a $S_{II}{}' \rightarrow S_{II}$ jump, leading to a net process $S_{I}{}' \rightarrow (S_{III}$ or $S_{III}{}')$. The preferred binding site in both Na−X and Na−Y involves HFCs anchored by both site II and site III′ cations. The loading dependence of the heat of HFC adsorption in zeolite Na−X is predicted to be different from that in Na−Y, because of the energetics of cation migration in Na−Y. HFC-134 is generally more strongly bound to both zeolites, because of its ability to make close Na−F and O−H contacts with the zeolites. The binding energy for the gauche conformer of HFC-134 is larger than that for trans at low loadings, but as loading increases, the difference decreases. The highly correlated small-amplitude motion predicted for cations in bare faujasites is quenched upon adsorption of HFCs. Most of the HFCs are too strongly bound to exhibit diffusive behavior during our molecular dynamics simulations.

I. Introduction

Hydrofluorocarbons (HFCs) have been identified as suitable substitutes for ozone depleting chlorofluorocarbons (CFCs). Specifically HFC-134a ($CH_2F−CF_3$) can substitute CFC-12 (CF_2Cl_2) as a coolant for air conditioning and refrigeration applications[1] and has no negative effect on the stratospheric ozone layer.[2] Synthesis of HFCs often leads to the production of isomers and impurities that may have to be separated in a subsequent step.[3,4] Effective separation of HFC mixtures such as HFC-134 ($CF_2H−CF_2H$) and HFC-134a has been achieved by use of cationic faujasites[5,6] such as Na−X and Na−Y, which are distinguished by their Si:Al ratio [Si:Al(X) < 1.5, Si:Al(Y) > 1.5] and consequently by their Na cation content. Zeolites have also been used to separate mixtures of HFCs and water.[7,8] During the study of the separation of HFCs isomers in Na−Y by combined NMR and X-ray techniques, Grey et al. observed significant migration of Na cations from site I′ into the supercage

and into the hexahonal prisms after adsorption of both HFC-134[9] and HFC-134a.[10] They suggested that the favorable HFC interaction with Na cations is optimized by this migration. Subsequent studies using [23]Na magic angle spinning (MAS) NMR, two-dimensional multiple quantum MAS NMR,[11] and in-situ X-ray powder diffraction[12] corroborated this interpretation. Although cation redistribution is expected in wet zeolites, such large amplitude motions are not usually observed in dry zeolite−guest systems. Another interesting experimental finding for this system is the preference for the gauche conformer of HFC-134 upon adsorption in the zeolite, in contrast to the higher stability of the trans conformer in gas phase[13−15] and the finding that the trans/gauche ratio depends on the HFC loading. In this paper, we apply molecular simulation techniques allowing simultaneous motion of Na cations and HFCs to explore the energetics and mechanisms of these surprising cation migrations in dry zeolites.

We have previously published a force field that accounts for the behavior of cations in dry faujasite-type zeolites.[16] This force field explicitly treats aluminum atoms as different from silicon atoms and makes no assumptions about occupancies in cation positions. We now extend the model to include HFC molecules

* To whom correspondence should be addressed. E-mail: auerbach@chem.umass.edu.
† Department of Chemistry, University of Massachusetts.
‡ SUNY Stony Brook.
§ Department of Chemical Engineering, University of Massachusetts.

adsorbed in zeolites. Several studies have been reported that model HFCs but almost all in liquid phase with no adsorbents[17-26] and only two studies in gas phase.[27,28] Ab initio calculations have also been performed for isolated HFC-134 and HFC-134a.[29-32] Relatively few computational studies have been reported for HFCs adsorbed in zeolites.[15,33-35] George et al.[33] applied a combination of Monte Carlo (MC) and molecular dynamics (MD) techniques to investigate the sorption of CFCs and HCFCs in zeolites using the CFF91 force field.[36] They kept fixed the zeolite framework and the extraframework cations and used an average T atom to account for Si and Al atoms. Mellot and Cheetham[34,37-39] developed a force field for small fluoro- and chlorofluorocarbons adsorbed in siliceous Y and Na−Y zeolites. They performed MC simulations using a Coulombic plus Lennard-Jones (12:6) potential keeping rigid the zeolite structure and also using the average T-site model. Recently, Lim et al.[35] performed energy minimizations and MD simulations to study binding energies and binding site geometries for HFC-134 and HFC-134a adsorbed in Na−X and Na−Y. Lim et al. kept cations fixed and used the average T-site model, preventing the observation of cation migration in Na−Y. Additionally, Crawford et al.[15] calculated HFC binding energies by ab initio density functional theory. To our knowledge, no force field is available that can accurately account for simultaneous large amplitude motion of cations and HFCs in zeolites.

The study of Lim et al. mentioned above involved a combined experimental and computational study of asymmetric HFCs on zeolites Na−X and Na−Y.[35] Double resonance NMR experiments indicated that HFC binding geometries are controlled by a balance between Na−F and O−H host−guest contacts. MD and simulated annealing calculations for HFC-134 and HFC-134a on model Na−X and Na−Y zeolites also revealed the importance of both H-bonding and Na−F interactions in determining the adsorption sites.

In the present paper, we develop a force field for HFCs in zeolites that can be used with various Si:Al ratios and different loadings of the adsorbate. It explicitly distinguishes Si from Al and different types of bridging oxygens while allowing cations and HFCs to move without preconceived constraints. We show below that our model reproduces experimentally observed heats of adsorption, geometries of the adsorption sites, conformer mix for HFC-134, vibrational frequencies, and interatomic distances found in the HFC−zeolite system. Our force field also accounts partially for the migration of cations, which has been observed experimentally. We do not observe full migration because Na−O cation−frame interactions compete effectively with the Na−F interactions, which are thought to pull Na cations into Na−Y supercages.

The remainder of this paper is organized as follows: In section II, we discuss the methodologies for force field development, system annealing, and dynamics. In section III, we discuss the results from our new force field with a focus on cation migration properties. In section IV, we give concluding remarks.

II. Methodology

As stated in the Introduction, the goal of this study is to develop a force field for exploring the simultaneous migration of cations and HFCs in faujasite-type zeolites, accounting for the binding of different HFCs in the zeolite and for the altered cation distributions that arise upon HFC binding. The force field has to be flexible enough to be used for zeolites with various silicon to aluminum (Si:Al) ratios and at different guest coverages, without the need for reparametrization each time a

TABLE 1: Calculated and Experimental Dipole Moments for HFC-134 and HFC-134A

species	experimental in gas phase	calculated in gas phase	calculated in zeolite
HFC-134a	2.06[a,b]	2.05	1.98
HFC-134 *trans*	0.00[c]	0.00	0.12
HFC-134 *gauche*	2.90[d]	2.90	2.82

[a] All values in Debyes. [b] Taken from Meyer and Morrison.[46] [c] By symmetry. [d] Taken from Mukhtarov and Kuliev.[48]

different system is considered. We fit the force field to experimentally determined heats of adsorption, dipole moments, HFC-134 conformer ratios, interatomic distances, and vibrational spectra, with an eye toward producing a model that allows for some cation migration. The resulting force field will be used to predict HFC and cation dynamics and to gain insights into the adsorption behavior of HFCs in dry zeolites and in the interesting phenomenon of cation migration.

There are some features in our model that make it different from previous approaches. In our previous paper,[16] we discussed the advantages of using different charges on silicon and aluminum, instead of an average T site when using mobile cations. Among them were the possibility of distinguishing different types of sites I′ and III′, the observation of site I cations off-centered in the hexagonal prisms,[40-42] and the more faithful accounting of the IR spectra.[43] The previous studies on modeling HFCs in zeolites[33-35] used the "average T-site" model and kept fixed the zeolite framework and the extraframework cations. In an effort to model the framework charge distribution more faithfully, we developed a force field that contains different partial charges on silicon and aluminum and that reproduces experimental data *without* constraining cations. We expect that this will provide a realistic model for cation and HFC dynamics in a variety of zeolites, enabling us to model the migration of cations that takes place upon adsorption of HFCs.

To construct a force field for HFC dynamics, we require atomic charges, short-range potential parameters, algorithms for calculating minimum energy configurations, ensemble averages and dynamics, and a method for classifying cationic sites. In what follows, we discuss each of these elements.

A. Atomic Charges. Details of the force field used for the framework atoms and extraframework cations are given in our previous paper.[16] Our model explicitly obeys Löwenstein's rule[44] forbidding two contiguous tetrahedral aluminum atoms in the structure. To have a portable force field that can be used for different Si:Al ratios, different charges were used for oxygen atoms bridging two silicon atoms (labeled O_s), and oxygens bridging one silicon and one aluminum atom (labeled O_a).

Atomic charges for HFCs were fitted to the measured dipole moments of each species of interest. As far as we know, a set of charges for HFC-134 and HFC-134a obtained by electronic structure calculations has not been reported. Charges obtained by ab initio methods for fluoromethanes range between −0.200 and −0.262 for fluorine and −0.020 and +0.049 for hydrogen,[17,26,45] whereas for fluoropropanes, Yamamoto et al.[22] obtained −0.30 for fluorine and +0.21 for hydrogen. On the basis of these results, we assigned $q_H = +0.1$ and fitted the values of q_F and q_C to match experimental dipoles in gas phase for HFC-134a[46,47] and HFC-134 gauche.[48] The calculated dipole moments of HFC-134a, HFC-134 trans, and HFC-134 gauche in gas phase and in the zeolite along with the experimental dipole moments are shown in Table 1, whereas the atomic charges used are shown in Table 2. The reason that HFC-134 trans has a calculated dipole moment different from zero is that after it is adsorbed in the zeolite the symmetry of the molecule

Cation Migration in Dry Zeolites

J. Phys. Chem. B, Vol. 105, No. 49, 2001 **12321**

TABLE 2: Partial Charges for the Zeolite and HFC Potential

species	partial charges	species	partial charges
Si	+2.050	C[c]	+0.250
Al	+1.750	C[d]	+0.525
$O_a{}^a$	−1.200	C[e]	−0.025
$O_s{}^b$	−1.025	H	+0.100
Na	+1.000	F	−0.175

[a] Oxygen bridging an Al atom and a Si atom. [b] Oxygen bridging two Si atoms. [c] Carbons in −CF$_2$H group of HFC-134. [d] Carbon in −CF$_3$ group of HFC-134a. [e] Carbon in −CFH$_2$ group of HFC-134a.

is broken. This broken symmetry for HFCs has also been observed in the gas phase[47,49] and has been calculated by ab initio methods.[29]

During the assignment of atomic charges, we enforced neutrality at each −CF$_2$H, −CF$_3$, and −CFH$_2$ group following the ab initio calculations of Yamamoto et al.[22] and Davis et al.[45] This assumption was also employed by Lísal et al.[24,25] although they used a different charge set for HFC-134 and HFC-134a. Some other charge sets that give acceptable values of HFC dipole moments were tested, producing either unsatisfactory fitting with other properties such as binding energies or fitting for just one type of guest molecule or for only a single Si:Al ratio. As seen in Table 2, our charge set for flouroethanes in zeolites is comparable with the ab initio values discussed above. In particular, the charge of +0.100 we use for hydrogen falls in the range observed in the gas phase for fluoromethanes and fluoropropanes and can also be justified by the enhanced polarization due to the formation of hydrogen bonds in the system.[10,35]

B. Potential. Several different force fields have been used to treat HFC intra- and intermolecular interactions, mostly in the gas phase; here, we briefly review some conformational properties these force fields must reproduce. HFC-134 has two different staggered conformers, trans (C_{2h} symmetry) and gauche (C_2 symmetry). In the gas phase, the trans conformer of HFC-134 is more stable by 4.9 to 10.0 kJ mol^{-1} than the gauche conformer[29,49−52] and there is an energy barrier for internal rotation of about 15−17 kJ mol^{-1}.[53] Hence, trans is the predominant conformer in the gas phase. In the liquid phase, the trans conformer of HFC-134 is more stable by about 1.7 kJ mol^{-1} than the gauche conformer.[50] In the crystalline state, only the trans configuration is present.[50] The dipole moments of the two conformers are very different[48] as shown in Table 1. This difference may also play a role during the process of HFC separation as has been suggested.[15] HFC-134a has only one staggered conformer (C_s symmetry), a dipole moment between the two conformers of HFC-134,[46] and an energy barrier for internal rotation of about 13.8 to 17 kJ mol^{-1}.[47,54,55] Upon adsorption in faujasites, gauche becomes the preferred conformer of HFC-134.[13−15] It has also been observed that, with increasing HFC-134 loading, the trans/gauche ratio increases and is independent of temperature.[15]

Here, we briefly review some of the force fields applied to model HFCs. Molecular dynamics has been performed to study thermodynamics and static structure of liquid HFC by Böhm et al.[17,18] using a potential derived from ab initio calculations and by Gough et al.[19] using the AMBER potential function.[56] Thermodynamic properties and diffusion were studied by Vega et al.[20] and Lísal et al.[21] using a homonuclear two-center Lennard-Jones potential with a dipole along the molecular axis, by Lísal et al.[23−25] using a Coulombic plus a Halgren's Buf 14−7 type potential,[57] and by Higashi and Takada[26] using a Coulombic plus Lennard-Jones (12:6) potential. Heublein et al.[27]

TABLE 3: Intramolecular Potential Parameters[a]

Quadratic Bond: $E = 1/2K(r − r_0)^2$

species	K (eV/Å^2)	r_0 (Å)
C−C	27.988	1.526
C−H	29.540	1.105
C−F	43.016	1.363

Quadratic Angle: $E = 1/2K(\theta − \theta_0)^2$

species	K (eV/rad^2)	θ_0 (degrees)
F−C−C	8.586	107.8
F−C−H	5.378	107.1
H−C−H	3.426	106.4
H−C−C	3.816	110.0
F−C−F	4.042	109.5

Torsion Angle: $E = K[1 + \alpha\cos\beta\phi]$

species	K (eV)	α	β
−C−C−	0.0617	1.0	3.0

[a] Taken from the Biosym/MSI CFF91 force field[36] and George et al.[33]

studied potential barriers for internal rotation in haloethanes using Buckingham and Lennard-Jones (12:6) potentials, and Fermeglia and Pricl[28] used the COMPASS 1.0 force field to study equations of state for HFCs. Monte Carlo simulations have been performed by Yamamoto et al.[22] using a Coulombic plus Lennard-Jones (12:6) potential to obtain thermodynamical properties of fluoropropanes. Mixtures of HFCs and hydrochlorofluorocarbons (HCFCs) have been studied by Gao et al.[58] at vapor−liquid equilibrium using an effective Stockmayer potential (Lennard-Jones 12:6 potential plus the potential between two point dipoles). All of these studies were conducted in the gas or liquid phase for pure HFCs. In general, these force fields give good to excellent agreement for different dynamical and thermodynamical properties of the systems.

As mentioned in the Introduction, there have been very few reports of modeling fluorocarbons in zeolites. George et al.[33] studied CFCs and HCFCs adsorbed in a variety of zeolites using the CFF91 force field,[36] whereas Mellot and Cheetham[34,37−39] studied the energetics and structures of small fluoro- and chlorofluoromethanes in Na−X and Na−Y using a Coulombic plus Lennard-Jones (12:6) potential. Lim et al.[35] studied energetics and geometries of HFC binding sites keeping cations in fixed positions. All of these studies used the average T-site model and fixed cations, preventing the simulation of cation migration.

Our force field includes parameters for the guest intramolecular and intermolecular interactions as well as parameters for the host−guest and host−host interactions. The guest intramolecular potential is based on the standard CFF91 molecular mechanics force field available from MSI.[36] This force field describes bonds and bond angles with harmonic functions and also includes a torsional potential as follows:

$$V_{intra} = \sum_{bonds} \frac{1}{2} K_b (r − r_0)_b{}^2 + \sum_{angles} \frac{1}{2} K_a (\theta − \theta_0)_a{}^2 + \sum_{torsions} K_t [1 + \alpha \cos \beta\phi]_t \quad (1)$$

The values of the parameters used for the intramolecular potential are given in Table 3 and are based on those used by George et al.[33]

The guest−guest and host−guest nonbonded interactions are represented by a Lennard-Jones (12:6) potential and a Coulomb

12322 *J. Phys. Chem. B, Vol. 105, No. 49, 2001*

Jaramillo et al.

TABLE 4: Parameters for Nonbonded Intermolecular Interactions

species	ϵ_{ij} (meV)	σ_{ij} (Å)	species	ϵ_{ij} (meV)	σ_{ij} (Å)
C−C[a]	1.691	4.350	H−Si	1.691	3.537
C−H	1.669	3.458	H−Al	1.691	3.537
C−F	2.246	3.878	H−O[b]	4.036	2.971
C−Si	1.713	4.448	H−Na	10.715	2.420
C−Al	1.713	4.448	F−F	2.982	3.457
C−O[b]	4.089	3.737	F−Si	3.554	3.822
C−Na	10.857	3.044	F−Al	3.554	3.822
H−H	1.648	2.750	F−O[b]	4.344	3.458
H−F	2.217	3.083	F−Na	30.013	2.176

[a] All parameters not involving F or Na were taken from the CFF91 force field.[36] [b] Same values used for both O_a and O_s.

TABLE 5: Cation-Framework Short-Range Buckingham Parameters

species	A (eV)	ρ (Å)	C (eV Å^6)
Na−O[a]	6230.0	0.2468	10.0

[a] Same values used both for O_a and O_s.

potential:

$$V_{\text{nonbond}} = \sum_{i,j>i} 4\epsilon_{ij}\left[\left(\frac{\sigma_{ij}}{r_{ij}}\right)^{12} - \left(\frac{\sigma_{ij}}{r_{ij}}\right)^{6}\right] + \sum_{i,j>i} \frac{q_i q_j}{r_{ij}} \quad (2)$$

The values of ϵ_{ij} and σ_{ij} were obtained by fixing the charges according to section IIA and varying ϵ_{ij} and σ_{ij} by trial and error until calculated distances and heats of adsorption agree semiquantitatively with experimental values. The starting values for these iterations were the nonbonded potential parameters in the standard CFF91 molecular mechanics force field.[36] As a further check of the potential, the Fourier transform of the dipole moment autocorrelation function was calculated to ensure that they agree qualitatively with experimental infrared spectra. The values of the potential parameters ϵ_{ij} and σ_{ij} for nonbonded interactions are summarized in Table 4.

The form of the cation-frame potential follows the one developed for zeolites by Catlow et al.,[59] involving two contributions: a Coulombic part and a Buckingham interaction between cations and oxygens. The Buckingham potential, which models repulsive and dispersive Na−O interactions, is given by

$$V_{\text{Buck}} = \sum_{i>j}\left[A_{ij}e^{-r_{ij}/\rho_{ij}} - \frac{C_{ij}}{r_{ij}^{6}}\right] \quad (3)$$

The interaction between cations and Si/Al atoms is described with a Coulombic term only, because the Coulombic repulsion between Na and Si/Al keeps them well separated and the polarizabilities of Si and Al are much less than that of oxygen. The values of the cation-frame potential parameters are summarized in Table 5. They differ only slightly from our published values for bare zeolites.[16] This small change does not affect the cation distributions obtained previously for bare Na−X and Na−Y and only increases slightly (less than 0.1 Å) the calculated Na−O interatomic distances. This new set of parameters is also more compatible with modeling HFC adsorption at high loadings, by producing a model that gives cation migration upon HFC adsorption while keeping other observables such as heats of adsorption, IR spectra, distances, etc., within experimentally reasonable ranges.

C. Annealing of Guest HFC Molecules. MD-DOCKER[60] is a simulated annealing procedure[61] that we used to obtain minimum energy configurations for HFCs and Na cations in zeolites. Our modeling considered the cases of 1 HFC/unit cell (zero loading or infinite dilution), 8 HFCs/unit cell (an average of 1 HFC/supercage), 16 HFCs/unit cell (an average of 2 HFCs/supercage), and 32 HFCs/unit cell (an average of 4 HFCs/supercage). In the cases of multiple HFCs/unit cell, we modeled in each simulation not only one conformer of HFC-134 but also mixtures of the two conformers. Calculations were performed with the program DIZZY[62] for Si:Al ratios of 1.2 (Na−X) and 2.4 (Na−Y). The modeling was performed in a faujasite unit cell containing in addition to the guest molecules n Al atoms, $192 - n$ Si atoms, $2n$ O_a atoms, $384 - 2n$ O_s atoms and n Na atoms, totalling $576 + n$ particles plus the guests atoms. For a Si:Al ratio of 1.2, $n = 86$, and for a Si:Al ratio of 2.4, $n=56$. The unit cell is cubic with a lattice parameter of ca. 24.8 Å.[63] Periodic boundary conditions are employed throughout via the periodic image convention. Short-range forces are cut off and shifted at 12 Å, and long-range forces are evaluated with the Ewald summation.[64]

Each annealing consisted of at least 100 independent energy minimizations. Each energy minimization was initiated by a minimum of 1000 steps of 1 fs molecular dynamics at 1000 K, followed by system cooling using the dynamical minimization algorithm LFOPC developed by Snyman.[65] Simulations were performed with both flexible and rigid zeolite framework, yielding essentially the same results. Different initial cation distributions were used to start the annealing procedure, to ensure proper sampling of very different cation configurations that may be separated by relatively large free energy barriers. For Na−Y (Si:Al = 2.4), these initial distributions are (a) 8 cations in site I, 16 in I′, and 32 in site II as observed in bare zeolite Na−Y by Eulemberger et al.[66] using X-ray powder diffraction and by Fitch et al.[63] using powder neutron diffraction; (b) 32 cations in site II and 24 in site III′, assuming that all cations are in the supercage; and (c) the minimum energy configuration found with our model for cations in bare zeolites,[16] i.e., 7 cations in site I, 17 in I′, 25 in II, 5 in II′, and 2 in site III′. In the case of Na−X (Si:Al = 1.2), the starting cation distributions are (a) 32 cations in site I′, 32 in site II, and 22 in site III′, assuming full occupancy of sites I′ and II, and placing the remaining cations in site III′ as observed by Vitale et al.[67] using neutron diffraction and used previously by Auerbach et al.[68] and by Lim et al.[35] and (b) the minimum energy configuration obtained with our model for cations in bare zeolites,[16] i.e., 1 cation in site I, 31 in I′, 32 in II, 7 in III, and 15 in III′. In the case of 1 HFC-134/unit cell, annealing was performed for each conformer, whereas at higher loadings, we started with an all gauche configuration and with a trans/gauche ratio of 1 placing the individual molecules randomly in the supercage of the zeolite.

D. Cation Classification Program. The extraframework cations in faujasites are located in various crystallographic positions, as shown in Figure 1. Site I cations are located in the hexagonal prisms, which connect sodalite cages (β cages). Site II cations are in the supercage, coordinated to three oxygens from the 6-ring window of a sodalite cage. Site I′ and II′ cations are inside the sodalite cage facing positions I and II, respectively. A unit cell of faujasite contains 16 possible sites I and 32 of each I′, II, and II′. Two additional sites have been found in the Na−X supercage: sites III and III′. Cations in site III are located above the 4-ring window, whereas those in site III′ are in different, but closely related, positions at the edges of the 4-ring window, i.e., in the 12-ring window.[69,70]

In an effort to compare our simulated cation locations to experimentally determined sites and occupancies, we created a
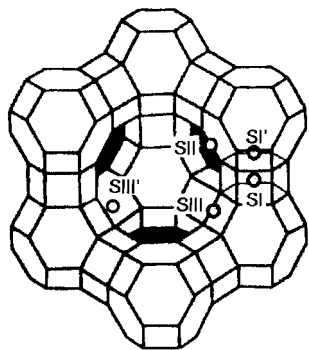
Cation Migration in Dry Zeolites

J. Phys. Chem. B, Vol. 105, No. 49, 2001 **12323**

Figure 1. Position of extraframework Na cations in faujasite-type zeolites Na−X and Na−Y.

program called CLAZYX (CLAssification for Zeolites Y and X) that converts three-dimensional coordinates into cationic sites. This program classifies cations based on their positions relative to other atoms, rings, and cages in the faujasite structure. The algorithm used in CLAZYX was given in our previous paper.[16]

E. Dynamics. We performed molecular dynamics calculations in order to study ensemble-averaged adsorption and diffusion properties of the HFCs, as well as the phenomenon of cation migration reported by Grey et al.[9,10] Dynamics were started from the minimum energy configuration positions obtained during the annealing procedure as well as from the initial configurations used for the annealing as described in section IIC. As in the case of the energy minimizations, the simulations were performed using the program DIZZY.[62] Molecular dynamics calculations were carried out in the canonical ensemble (*NVT*) using the Nosé−Hoover chain method of Martyna et al.[71−73] following the Jang and Voth algorithm[74−77] with a chain of four thermostats. We used full periodic boundary conditions and a simulation cell containing one unit cell of faujasite (576 atoms) plus the extraframework cations and the guest molecules.

We performed dynamics for 1, 8, 16, and 32 HFCs/unit cell. In the cases of multiple HFCs/unit cell, we also ran dynamics in which all of the guest HFC-134 molecules were initially of the same conformer in order to observe the evolution of the conformer ratio toward the equilibrium values observed by Crawford et al.[15] Simulations were performed at a temperature of 300 K, using a 1 fs time step and Si:Al ratios of 1.2 and 2.4. Total simulation times were at least 500 ps. Cation and HFC coordinates and velocities were recorded at least every 50 steps, as well as coordinates for the center of mass of each guest molecule. The total dipole moment of the system was calculated at least every five steps. Cation sites and jumps were monitored every 10 steps. Histograms showing the extent to which cation motion is correlated were constructed from these data. Mean square displacements were calculated for each HFC from the displacement of their center of mass. The densities of vibrational states were computed by Fourier transformation of velocity autocorrelation functions. The infrared spectrum for the system was calculated by Fourier transformation of the dipole moment autocorrelation function using a Blackman window and scaling factor as outlined by Berens and Wilson.[78]

III. Results and Discussion

The force field we have developed was used to model HFC-134 and HFC-134a at different loadings in faujasites with Si:Al ratios of 1.2 and 2.4. Below we compare the results of our simulated annealing and MD against experimental data for cation site occupancies, heats of HFC adsorption, HFC binding site

TABLE 6: Net Number of Cations that Migrate to the Supercage upon the Adsorption of HFCs in Na−Y

HFC coverage/u.c.	simulation				experimental[11]	
	1	8	16	32	16	32
HFC-134a	0	1	8	10		
HFC-134	0[a]	2	7	11	15 ± 3	13 ± 3

a Both conformers.

geometries, interatomic distances, and conformer ratios for HFC-134. We also report mean square displacements of guest molecules, vibrational spectra, and the mechanisms of cation migration. Although our *ultimate* goal is to explore the cation migration in Na−Y, we begin below by describing the cation distributions from our calculations, for use in later discussions of HFC binding on those cation distributions.

A. Cation Site Occupancies. Cation site occupancies were calculated with our program CLAZYX in order to investigate cation migration in zeolites. This phenomenon consists of the migration of cations of Na−Y from site I′ in the β cages to sites in the supercages (III and III′), upon the adsorption of HFC-134 or HFC-134a. This effect has not been detected in Na−X, probably because the supercage sites are already occupied in the bare zeolite; the optimization of the cation−HFC interactions thus proceeds without further rearrangment of the cation distribution. The number of cations that migrate increases with increasing HFC loading level. This phenomenon has been observed by both X-ray powder diffraction[9,12] and MAS NMR spectroscopy.[10,11] The migration is presumably the result of strong attractions between guest fluorine atoms and zeolite sodium cations. These Na−F attractions compete against strong Na−O (β cage) attractions. Depending on the balance between these competing interactions, one might expect partial migration. Despite this, Grey et al. have reported observations of complete Na(I′) migration in Na−Y upon adsorption of 16 HFCs/u.c.

In what follows, we compare our simulated cation migration patterns with previously published NMR data[11] but not with previous X-ray data[9] because of difficulties in interpreting these data. The net number of cations that migrate to the supercage calculated from our minimizations of HFCs in Na−Y is shown in Table 6. The results are independent of the cation configuration used to start the minimizations when at least 100 annealing cycles are performed. At low loadings, the favorable Na−F interaction is not strong enough to pull out cations from the β cages, so the cation configuration is similar to the one for the bare Na−Y as observed experimentally.[12] As guest coverage increases, these interactions become strong enough to drive cations to migrate toward the supercage. Our model predicts that seven cations migrate to the Na−Y supercage when 16 HFCs/u.c. adsorb, whereas NMR measurements observe 15 ± 3 new supercage cations. As such, we do not predict cation migration to the extent seen experimentally at 16 HFCs/u.c. However, at loadings of 32 HFCs/u.c., simulation and experiment are in better agreement; the former predicts 11 new supercage cations, whereas the latter observes 13 ± 3 new cations. Our results also show, in qualitative agreement with experiment,[10] that, although more cations migrate when HFC-134 is adsorbed than when HFC-134a is adsorbed, this difference is not large. Our simulations do not account, however, for the increased population in site I observed after migration by ^{23}Na MAS NMR.[11]

Generally, these results indicate that cation migration is essentially complete at a loading of 16 HFCs/u.c. This can be understood as follows: the maximum migration produces ca. two new cations per supercage, enough to tether two HFCs at
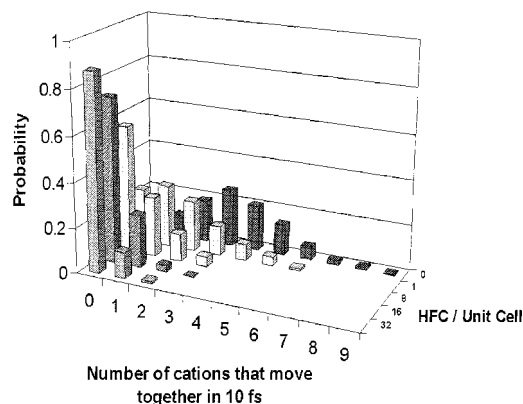
12324 *J. Phys. Chem. B, Vol. 105, No. 49, 2001*

Jaramillo et al.

Figure 2. Histogram indicating the extent of correlated cation motion, by counting number of jumping cations in a 10 fs interval for different loadings of HFC-134a in Na−Y (Si:Al = 2.4) at 300 K.

both ends. Because of steric constraints, the adsorption of new HFCs at higher loadings cannot pull additional cations into supercages, because there is not enough room (surface area) to support additional sites anchored by two cations.

The mechanism of cation migration was studied with our MD calculations. In the simulations of the HFC−zeolite system that started with the cation configuration for bare zeolite Na−Y (8 I, 16 I′, and 32 II; or 7 I, 17 I′, 25 II, 5 II′, and 2 III′), cation migration reached the minimal energy configuration after less than 150 ps for high loadings of both HFC-134 and HFC-134a. In all of the MD trajectories studied, the migration was found to be a concerted movement of cations from different sites as follows: initially, a cation in site I′ moves to an empty site II′ in the same β cage; simultaneously, the cation occupying the site II in the supercage directly across this site II′ moves to an adjacent site III or III′. In a later step, the cation in site II′ crosses the six-member ring dividing the β cage and the supercage, becoming a site II cation. The net effect of this concerted movement is the migration of a cation from site I′ to a site III′, although the cation that was originally in site I′ ends up in site II and the one in site II is finally in site III′. Evidence of site II to site III/III′ cage rearrangement in the Na−Y/HFC-134 system has been observed in gas sorption experiments by X-ray diffraction and MAS NMR.[79]

The cation migration mechanism is also consistent with our previous finding of small-amplitude concerted movement of cations in zeolites,[16] although the presence of the guest HFCs quenches most of this small-amplitude cation movement after the initial migration is over. Figure 2 shows a comparison of the concerted cation movement seen in bare zeolite Na−Y to that seen in the same type of zeolite after the adsorption of HFC-134a at different loadings. In our previous study of cation dynamics in bare zeolites, we observed many small-amplitude motions of several cations occurring in a highly concerted fashion. As an example, several cations would simultaneously vibrate from I↔I′, II↔II′, and III↔III′ sites. These motions appear in Figure 2 for bare zeolites with a peak at 4; that is, many cation vibrations involve the cooperative motion of 4 cations. From Figure 2, it is clear that, after cations have migrated from the β cage to the supercage upon HFC adsorption, the presence of guest molecules restricts further motion. This can be seen from the displacement of the highest bar in the histogram toward lower numbers with increasing loading of HFC. A similar behavior was observed when HFC-134 was adsorbed in Na−Y and also for Na−X with both types of HFC guests. Evidence of this small-amplitude motion through a six-membered ring was obtained by ^{23}Na MAS NMR in bare Na−Y

TABLE 7: Experimental and Simulated Values of Heat of Adsorption for HFCs in Na$_{86}$X

HFC coverage/u.c.	simulation				experimental[15,81]		
	1	8	16	32	1	16	32
HFC-134a	78.4^a	70.3	68.1	65.7	65	63.5	62
HFC-134	84.0^b	78.6	75.8	70.0	78	71	65
	77.2^c						

^{a} All values in kJ mol^{-1}. ^{b} gauche conformer. ^{c} trans conformer.

TABLE 8: Experimental and Simulated Values of Heat of Adsorption for HFCs in Na$_{56}$Y

HFC coverage/u.c.	simulation				experimental[11,12,80]	
	1	8	16	32	low	high
HFC-134a	67.2^a	55.4	61.4	63.8	57	57
HFC-134	71.8^b	62.9	67.1	66.4	69	59
	65.9^c					

^{a} All values in kJ mol^{-1}. ^{b} gauche conformer. ^{c} trans conformer.

and in Na−Y/HFC-134 systems, although at a much lower frequency of vibration than obtained in our simulations.[79]

B. Heats of Adsorption and Adsorption Site Geometry. Heats of adsorption were calculated from MD averages for HFC-134a and HFC-134 at different loadings in both Na−X and Na−Y. Heats of adsorption are compared with experiment to help validate the model; these heats also provide insights regarding the loading dependence of adsorption. The heat of adsorption in each case was calculated by subtracting from the energy of the HFC−zeolite system the energy of the bare zeolite and isolated HFCs:

$$\Delta U_{ads} = \langle V_{z+g} \rangle - (\langle V_z \rangle + \langle V_g \rangle) \qquad (4)$$

where ΔU_{ads} is the calculated heat of adsorption at constant volume, $\langle V_{z+g} \rangle$ is the average potential energy of the zeolite−guest system, $\langle V_z \rangle$ is the average potential energy of the bare zeolite, and $\langle V_g \rangle$ is the average potential energy of the guest molecules in gas phase; all of these energies are averaged at the same temperature.

In the case of infinite dilution (1 HFC/unit cell), we performed calculations for individual conformers of HFC-134. The results are shown in Table 7 for HFCs in Na−X and Table 8 for HFCs in Na−Y. For HFC-134 and HFC-134a adsorbed in zeolite Na−X, our results follow the experimentally observed trend of decreasing binding energy with increasing coverage. This can be explained on the basis of different adsorption sites available for HFC binding, as observed by Lim et al.[35] HFCs will bind first to the adsorption sites with the highest binding energy. At higher loadings, the preferred sites are already occupied and lower energy sites become populated. The calculated differences in heats of adsorption between HFC-134 and HFC-134a at different loadings in zeolite Na−Y are in good agreement with experiments. At high loadings, the heat of adsorption of HFC-134 in Na−Y is measured to be about 2 kJ mol^{-1} higher than for HFC-134a, whereas at loadings below 26 HFC/u.c., this difference is measured to be between 5 kJ mol^{-1}(medium loading) and 12 kJ mol^{-1} (low loading),[6,12,80] which compares well with our calculated values shown in Table 8.

Savitz et al.[81] estimated the contributions to the heat of adsorption from electrostatic and dispersive energy by comparing isosteric heats of adsorption of cationic and acidic zeolites. They found that the dispersion energy contribution to the isosteric heat of adsorption is constant (approximately 35 kJ

Cation Migration in Dry Zeolites

J. Phys. Chem. B, Vol. 105, No. 49, 2001 **12325**

TABLE 9: Contributions of Different Interactions to the Heat of Adsorption of HFC-134 in Na−Y

	16 HFC/u.c.	32 HFC/u.c.
Δ guest−guest total	−8.31[a]	-11.32
Δ cation−cation total	−9.72	-16.87
Δ cation−oxygen dispersive	−3.92	-5.60
Δ cation−oxygen electrostatic	+23.49	+38.20
Δ trans → gauche energy	+3.43	+2.66
Δ host−guest dispersive	−27.13	-26.17
Δ all other contributions[b]	−44.94	-47.30
Heat of Adsorption[c]	−67.10	-66.40

[a] All values in kJ mol^{-1}. [b] Included here are host−guest electrostatics and cation−Si/Al interactions. [c] Constant volume heat.

mol^{-1}) for both HFCs in Na−X and Na−Y. Our calculations also show a constant value of around 31 kJ mol^{-1} for the dispersive contribution in all of the systems. This is explained by the similar positioning of oxygens in the frameworks of both types of faujasites. It can also be noticed that, at low coverages, the binding energies for HFC-134a and the two conformers of HFC-134 follow the same trend as their dipole moments,[15,81] albeit extremely weakly. As a result, the differences in heats of adsorption come from different electrostatic contributions: to some extent from ion−dipole host−guest interactions, but to a large extent from other electrostatic interactions such as host−guest hydrogen bonding, which have been observed in this and other studies.[34,35,37−39]

In Table 9, we present the contributions from different interactions to the heat of adsorption of HFC-134 in Na−Y at high loadings. It can be seen that the predominant contribution to the HFC heat of adsorption is the large host−guest interaction, which has an electrostatic and a dispersive component. In HFC-134 at loadings of 2 HFCs/unit cell or greater, the electrostatic component is predicted to account for about 60% of the total host−guest interaction. There are, however, other important contributions that increase heats of adsorption, namely, (i) the decrease in Na−Na electrostatic repulsion in the supercage relative to the β cage because of the increased Na−Na distances resulting after cation migration, (ii) favorable guest−guest interactions, and (iii) the decrease in Na−O repulsion arising from increased Na−O distances. In the HFC-134−faujasite systems considered here, there are two contributions that decrease the predicted heats of adsorption, namely, (i) the trans to gauche interconversion energy, which is larger at low loadings because the trans/gauche ratio loading dependence and (ii) the decrease in electrostatic Na−O attraction resulting from cation migration. This attraction is significantly smaller in site III′ in comparison to that in site I′, the preferred site in bare Na−Y. In order for migration to take place, this large energetic price has to be paid, which is achieved by the large host−guest interaction in the supercage. As a result, the cation arrives at a site III′ where it has less electrostatic attraction with the coordinating oxygens. The energetic contributions to the heat of adsorption of HFC-134a in Na−Y are very similar to those of HFC-134 but without the trans to gauche interconversion energy.

In Na−X, where no cation migration takes place, the calculated heat of adsorption is due mainly to the adsorption site binding energy with a small contribution from the guest−guest interaction. The small changes in Na−O distances in the existing sites contribute only marginally to the heat of adsorption. Savitz et al.[81] obtained a difference of 12 kJ mol^{-1} between the heats of adsorption of HFC-134 and HFC-134a at the limit of zero coverage in Na−X at 298 K. This value compares reasonably well with our calculated value of about 6 kJ mol^{-1} at 300 K.

For HFCs adsorbed in Na−Y, our simulated heats appear to overestimate experimental values[11,80,81] as shown in Table 8. The large value of adsorption heat at low coverage is due to the HFC adsorbed in a site which is bound at one end to a site II cation and at the other end to a site III′ cation. Our previous results[16] predict that there is a small (but nonzero) number of site III′ cations in bare Na−Y; at low HFC coverages and low temperatures, HFCs are adsorbed at this preferred binding site. At higher temperatures, the HFC frequently samples higher energy sites, and for that reason, its heat of adsorption may be lower at those temperatures. *When HFC coverage is increased, cations migrate to the supercage providing more preferred adsorption sites, although not enough for each HFC.* This explains the predicted nonmonotonic loading dependence of HFC adsorption heats in Na−Y shown in Table 8; that is, the initial heat is large for the reasons stated above. The heat then drops as preferred sites fill but then increases again as cations migrate. Guest molecules that cannot bind to two cations will adsorb at sites with only one cation. No matter the position and number of achoring cations, hydrogen atoms from the HFCs interact with the zeolite framework through hydrogen bonds, as shown by Lim et al.[35] The presence of strongly electronegative F atoms in the HFC increases the acidity of the H atoms and thereby enhances their tendency to form hydrogen bonds.

At very high HFC coverages, the migration of cations to the supercage will make the cation environment in the supercage of Na−Y resemble that of Na−X, with multiple site III′ cations available as adsorption sites for HFCs. For this reason, the simulated heats of adsorption in Na−Y at high coverages increase and start resembling those of Na−X. The difference in the heats of adsorption between gauche HFC-134 and HFC-134a in both Na−X and Na−Y is noteworthy. This difference has been proposed as that responsible for HFC separation.[15] Our calculations show that at low coverages, the gauche conformer of HFC-134 would be more strongly bound to the zeolite than HFC-134a (see section IIID). The competition for the scarce strongly binding sites is won by HFC-134 gauche.

With respect to the geometry of the adsorption sites in Na−X, our results are consistent with the findings of our recent paper,[35] in which a detailed account of the different adsorption sites is given. In that paper, which focused on low HFC loadings, cations were kept fixed preventing the observation of cation migration. With our current force field, partial migration of cations from the β cages to the supercages has been observed in Na−Y. The resulting distribution of cations in the supercage of Na−Y at high HFC loadings resembles that of Na−X. For that reason, similar binding sites are observed in both zeolites in the present study. In the preferred sites, the HFCs are coordinated with two cations by Na−F interactions, one in site II an other in site III′, and by O−H interactions. This binding site is shown in Figure 3.

When loading increases, the guest molecules are forced to adsorb at sites that have lower binding energies involving coordination with only one cation. Besides the sites coordinating one zeolite cation with one fluorine from the guest molecule, we have found sites that have fluorine atoms from different ends of the HFC coordinating with one cation and even some sites that have host−guest coordination through O−H bonding only.[35] Thus, at high HFC loading in Na−Y the binding sites available are similar to those in Na−X, because of the cation distributions that arise after HFC-induced migration.

C. Interatomic Distances. Selected distances from cations to framework oxygens and to fluorine atoms of the guest molecules are shown in Table 10 for bare Na−Y and for Na−Y

TABLE 10: Selected Interatomic Distances in Bare Na−Y and in Na−Y after the Adsorption of HFC-134

	bare Na−Y		16 HFC-134/u.c.		32 HFC-134/u.c.	
species	experiment[9,a,b]	simulation	experiment[9]	simulation	experiment[9]	simulation
Na(I)-O(3)[c]	2.71	2.18−2.34	2.54	2.22−2.33	2.62	2.20−2.35
Na(II)-O(2)	2.33	2.21−2.42	2.48	2.32−2.50	2.51	2.31−2.50
Na(II)-O(4)	2.89	2.68−2.89	3.17	2.86−3.14	3.25	2.91−3.19
Na(III′)-O(1)			3.12	2.74−3.07	3.06	2.72−3.06
Na(III′)-O(4)			2.71	2.59−2.75	2.71	2.57−2.74
Na(II)-F(4)			2.72	2.51−2.68	2.71	2.50−2.69
Na(III′)-F(1)			2.70	2.53−2.67	2.70	2.50−2.67
Na(III′)-F(2)			3.26	3.11−3.29	3.25	3.12−3.31
Na(III′)-F(3)			3.09	2.89−3.07	3.38	2.91−3.09

[a] All distances in angstroms. [b] Experimental results taken at 100 K. [c] Atom labels follow Grey et al.[9]
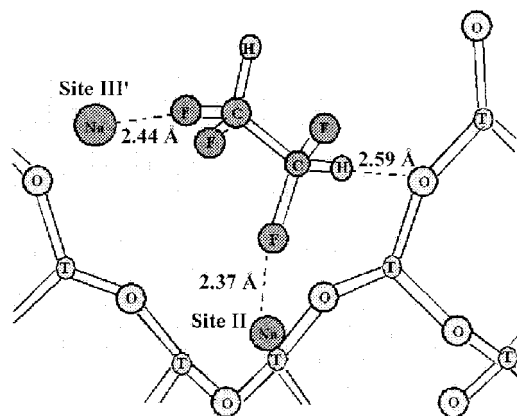
Figure 3. Preferred binding site for HFC-134 gauche in Na$_{56}$Y.

with HFC-134 adsorbed at coverages of 16 and 32 guest molecules per unit cell. Our results for interatomic distances show a range rather than a single value because each roughly equivalent cation is in a slightly different environment because of the different arrangement of framework Si and Al in its proximity. Similarly, the guest HFCs are present in diverse binding sites. In the case of the bare zeolite Na−Y, the distances are essentially identical (within 0.1 Å) to those found in our previous study of cations in zeolites,[16] despite the small change in the potential parameters for the Na−O interaction. As was pointed out in that paper, the agreement is excellent with the exception of the Na(I)−O(3) distance. The site I is often reported by experiments to reside in the center of the hexagonal prism.[9,63,66,82] Our results suggest that Na(I) is not located at the center of the hexagonal prism but rather is in one of two symmetric site I displaced by about 0.6 Å along the [111] direction. This qualitative displacement has been observed by Engelhardt[41] using DOR ^{23}Na NMR and further observed by synchrotron X-ray powder diffraction for Zn cations in zeolite X.[42]

As observed by Grey et al.[9] using X-ray powder diffraction, a significant increase of the Na(II)−O distance is calculated in our model after adsorption of 16 or more guest molecules per unit cell. This is due to the pulling effect exerted by the fluorine atoms present in the HFCs. This same pulling effect can be credited, as said before, for the cation migration observed. As in the case of experiments, our simulations do not find a large difference between the cation−oxygen distances at different HFC loading levels. Although the present model gives Na−F distances that are slightly shorter than those observed in the experiment, the level of agreement is generally very good, especially given the errors associated in the structural refinement of these highly correlated systems.

D. HFC-134 Conformer Ratio. Using our force field for HFC-134 in the gas phase, a difference of 6.1 kJ mol^{-1} is

calculated between the more stable trans conformer and the gauche conformer. The calculated energy barrier for internal rotation is 17.8 kJ mol^{-1}. These values fall well into the experimentally obtained ranges of 4.9−10.0 kJ mol^{-1} for the difference in energy between conformers[29,49−52] and the value of 15−17 kJ mol^{-1} for the energy barrier for internal rotation.[53] As can be seen in Tables 7 and 8, HFC-134 gauche is energetically preferred to trans in faujasites at low coverage. This behavior can be ascribed to a more effective configuration that minimizes Na−F distances and facilitates O−H bonding.[14,15] The gauche conformer can have all of its C−H bonds directed toward the surface of the zeolite, favoring the formation of hydrogen bonds.[14] A typical hydrogen bond has an energy of 12−21 kJ mol^{-1},[83] which is sufficient to overcome the energy barrier for rotation between conformers. When minimizations at low coverage are started with the trans conformer, we find that it converts to the gauche configuration in fewer than 40 annealing cycles. The opposite process is not observed. When the minimizations are performed at higher coverages, the final trans/gauche ratio is the same despite starting from configurations of different trans/gauche ratios, even starting from an all-gauche configuration.

In the case of 8 HFC-134 per unit cell (1 per supercage), minimizations that start with all guest molecules in either trans or gauche conformation yield similar results with a final trans/gauche = 0.3. At higher HFC loadings, when different initial ratios for trans/gauche conformers are used, the minimum energy structures found have a similar trans/gauche ratio. In the cases of 16 and 32 HFC-134 molecules per unit cell, the minimum energy configuration trans/gauche ratios are 0.8 and 1.3, respectively. Crawford et al.[15] observed a similar behavior using Raman spectroscopy. In this work, we have followed the trans/gauche ratio by simulating the loading dependence of the IR spectra of HFC-134 at 300 K (see section IIIF). This observed change in conformer mix can also help to explain the decrease in binding energy with increasing guest coverage, because of the lower binding energy associated with the trans conformer.

E. Mean Square Displacement of Cations and HFCs. Mean square displacements (MSD) were calculated from our MD runs for cations and for the centers of mass of individual HFCs. At 300 K, no appreciable motion is observed for cations in the MD calculations that started from the minimal energy configurations. In the case of HFCs, most of the guest molecules are fixed at the binding sites, and only a few are able to migrate to other sites in the same supercage or to adjacent supercages. The MSDs observed for the same loading of HFCs adsorbed in zeolites of different Si:Al ratios are not significantly different, which indicates that, despite the larger number of cations in Na−X, the sites available for HFC adsorption are similar.

At infinite dilution, MD simulations of HFCs in Na−X and Na−Y show that the trans conformer of HFC-134 is more
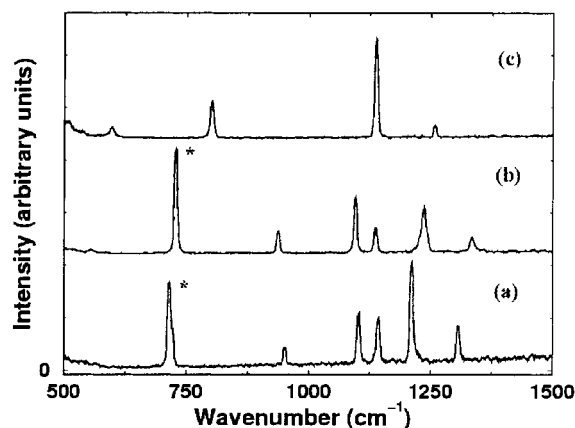
Cation Migration in Dry Zeolites

J. Phys. Chem. B, Vol. 105, No. 49, 2001 **12327**

Figure 4. Simulated infrared spectra of HFCs in Na$_{86}$X at 300 K at infinite dilution. (a) HFC-134 trans, (b) HFC-134 gauche, and (c) HFC-134a. The peaks marked with an asterisk are used in Figure 5 to follow the trans/gauche conformer ratio in HFC-134.

Figure 5. Simulated infrared spectra of HFC-134 in Na$_{86}$X at 300 K at different loadings. (a) trans conformer at infinite dilution (1HFC/u.c.), (b) gauche conformer at infinite dilution (1HFC/u.c.), (c) 8 HFC/u.c., (d) 16 HFC/u.c., and (e) 32 HFC/u.c.

mobile than either the gauche conformer or HFC-134a. HFC-134 trans jumps from site to site, anchoring to cations in sites II or III′ and changing at each jump the carbon end by which it is bound to the zeolite. These jumps are not restricted to one supercage, as jumps toward cations in adjacent supercages were observed. This site-to-site jump is somewhat larger in Na−X than in Na−Y. HFC-134 gauche also exhibits the same behavior but with a lower jump rate. HFC-134a has a jump rate intermediate between the two conformers of HFC-134. In this case, each jump changes the nature of the binding site, because its two ends are asymmetric. These observations are in qualitative agreement with those found by Lim et al.,[35] despite the different cation arrangement used by these authors.

F. Vibrational Spectra. IR spectra of the host−guest systems were calculated by Fourier transform of the dipole moment autocorrelation function using a Blackman window and a scaling factor.[78] The resulting spectra for HFCs adsorbed at infinite dilution in Na−X in the region of 500−1500 cm^{-1} are shown in Figure 4. To our knowledge, the IR spectra for these systems have not been published, and comparisons can only be made against spectra for bare zeolites or for gas-phase HFCs. In the region from 100 to 500 cm^{-1} the spectra are very confusing with multiple and broad bands due to zeolite absorption that are difficult to assign individually.[84−86] The assignment for HFC absorptions is somewhat easier, because of the sharper and more differentiated peaks. On the basis of published data,[87−91] we can assign the following peaks in the spectrum of HFC-134a shown in Figure 4: CF$_3$ symmetric deformation (597 cm^{-1}), CF$_3$ symmetric stretch (801 cm^{-1}), C−F stretch (1138 cm^{-1}), and CH$_2$ wag (1259 cm^{-1}). All of these values are slightly shifted (less than 40 cm^{-1}) toward lower wavenumbers compared to those of the gas-phase spectra, which is expected as an effect of the binding to the zeolite. Also, this binding may restrict some modes more than others producing a change in the relative intensities of the peaks.

On the basis of experimental data for gas-phase HFC-134,[50,52,92] we can assign the peaks for its two conformers. For HFC-134 gauche, we find CF$_2$ wag (728 cm^{-1}), C−C stretch (938 cm^{-1}), CF$_2$ stretch (1096, 1139, and 1237 cm^{-1}), and C−H bend (1337 cm^{-1}). For HFC-134 trans, we assign CF$_2$ wag (713 cm^{-1}), C−C stretch (951 cm^{-1}), CF$_2$ stretch (1103, 1143, and 1211 cm^{-1}), and C−H bend (1306 cm^{-1}). As in the case of HFC-134a, the peaks are shifted toward lower wavenumbers and with altered relative intensities compared with those of the gas-phase spectra. For all systems studied, a double peak at
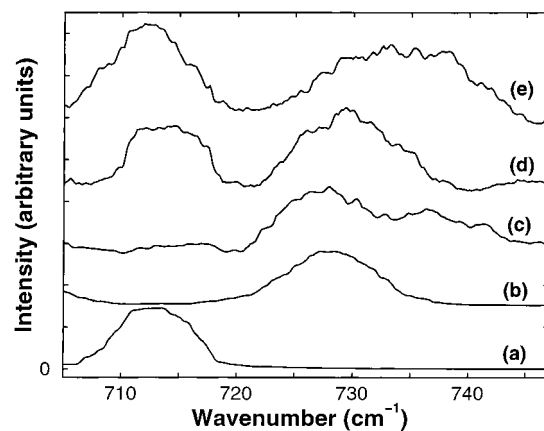
about 3050 cm^{-1} is observed because of the C−H stretch. This peak is broader than the corresponding gas-phase peak; this broadening has been attributed to the perturbation of the C−H vibration which is due to the formation of (relatively weak) hydrogen bonds between the C−H group and the oxygen ions in the zeolite framework.[14]

The differences in the IR spectra of the two conformers of HFC-134 and its loading dependence can be used to follow the trans/gauche conformer ratio, as has been done by Crawford et al.[13−15] using Raman spectroscopy. In Figure 5, we show that dependence by following the CF$_2$ wag vibration for HFC-134 at 300 K. The IR signals for trans and gauche conformers are clearly distinguishable, as shown in Figure 5 parts a and b. At the low loading of 8 HFC/u.c., only the gauche signal appears, as shown in Figure 5c. As loading increases, the relative sizes of the trans and gauche peaks indicate a significant emergence of the trans conformer, consistent with our previously discussed results in section IIID. These results can be used in principle to relate the trans/gauche IR intensity ratios with the trans/gauche population ratios, given the oscillator strengths of the two conformers.

IV. Conclusions

In this paper, we addressed some fundamental questions about the energetics and dynamics in hydrofluorocarbon (HFC) faujasite systems. Among these questions were, What is the contribution of individual interactions to the heat of adsorption of HFCs in zeolites? Why do heats of adsorption of HFCs in Na−X decrease with increasing guest loading? What is the role of the heat of adsorption in the separation of isomeric HFCs? Why is the gauche conformer of HFC-134 preferred upon adsorption in faujasites? What are the reasons and mechanisms for the observed cation migration? What are the dynamics of HFCs adsorbed in zeolites? To answer these questions, we applied different computational techniques, such as molecular dynamics and simulated annealing, to several zeolite−HFC systems varying in Si:Al ratio and loading of guest molecules.

We have developed and applied a new force field for simultaneously modeling the dynamics of HFCs and exchangeable Na cations in faujasite-type zeolites. Energy minimizations and molecular dynamics simulations performed with this force field give excellent agreement with experimental data on heats of adsorption, guest−host distances, infrared spectra, and conformer ratios for different coverages of HFC-134 (CF$_2$H−CF$_2$H) and HFC-134a (CH$_2$F−CF$_3$) in Na−X (Si:Al = 1.2) and

Na–Y (Si:Al = 2.4). The force field also accounts for the observed cation migration partially at intermediate loadings and fully at high loadings. The extent of migration is found to be influenced by the competition among Na–O, Na–F, and Na–Na interactions. The Na–O interaction disfavors migration because Na(I′) sites are found to be energetically more favorable than Na(III′) sites; the Na–F attraction obviously favors migration; and surprisingly, the Na–Na repulsion also favors migration because moving Na cations into supercages leads to better cation dispersion. This migration occurs in a two-step mechanism that involves first a concerted two-cation jump, $S_{I'}$ → $S_{II'}$/S_{II}→(S_{III} or $S_{III'}$), followed by a $S_{II'}$ → S_{II} jump, leading to a net process $S_{I'}$ → (S_{III} or $S_{III'}$).

The preferred binding site in both Na–X and Na–Y involves HFCs anchored by both site II and site III′ cations. The loading dependence of the heat of HFC adsorption in zeolite Na–X is predicted to be different from that in Na–Y, because of the energetics of cation migration in Na–Y. HFC-134 is generally more strongly bound to both zeolites, because of its ability to make close Na–F and O–H contacts with the zeolites. The binding energy for the gauche conformer of HFC-134 is larger than that for trans at low loadings, but as loading increases, the difference decreases. The highly correlated small-amplitude motion predicted for cations in bare faujasites is quenched upon adsorption of HFCs. Most of the HFCs are too strongly bound to exhibit diffusive behavior during our molecular dynamics simulations.

To obtain more complete understanding for these systems in the future, improvements in three areas have to be achieved: energetics, dynamics, and experimental. In the energetics part, embedding techniques mixing quantum and classical energy calculations may be required to model the Na–O and Na–F interactions accurately enough to determine whether partial or full cation migration is predicted. To improve the dynamics and to quantify statistically meaningful time scales and activation energies of cation migration, techniques such as hyperdynamics[93,94] or transition path sampling[95–97] will be required to sample the many-body rare events. Single crystal diffraction experiments of cation migration may be required to measure more accurately partial occupancies in low symmetry cation sites.

References and Notes

(1) Manzer, L. E. *Science* **1990**, *249*, 31.
(2) Ravishankara, A.; Turnipseed, A.; Jensen, N.; Barone, S.; Mills, M.; Howard, C.; Solomon, S. *Science* **1994**, *263*, 71.
(3) Manzer, L. E.; Rao, V. N. M. *Adv. Catal.* **1993**, *39*, 329.
(4) Webb, G.; Winfield, J. *Chem. Brit.* **1992**, *28*, 996.
(5) Corbin, D. R.; Mahler, B. A. World Patent, W.O. 94/02440, 1994.
(6) Corbin, D. R.; Mahler, B. A. U.S. Patent 5,600,040, 1997.
(7) Soffer, A.; Agam, G.; Bar-Nes, G.; Boxer, D.; Dagan, G.; Gilron, J.; Kleiner, L.; Krakov, V. World Patent, W.O. 98/32521, 1998.
(8) Cohen, A. P.; Tucker, D. M. *ASHRAE Trans.* **1998**, *104*, 396.
(9) Grey, C. P.; Poshni, F. I.; Gualtieri, A. F.; Norby, P.; Hanson, J. C.; Corbin, D. R. *J. Am. Chem. Soc.* **1997**, *119*, 1981.
(10) Lim, K. H.; Grey, C. P. *Chem. Commun.* **1998**, 2257.
(11) Lim, K. H.; Grey, C. P. *J. Am. Chem. Soc.* **2000**, *122*, 9768.
(12) Ciraolo, M. F.; Hanson, J. C.; Norby, P.; Grey, C. P. *J. Phys. Chem. B* **2001**, *105*, 2604.

(13) Udovic, T. J.; Nicol, J. M.; Cavanagh, R. R.; Rush, J. J.; Crawford, M. K.; Grey, C. P.; Corbin, D. R. *Mater. Res. Soc. Symp. Proc.* **1995**, *376*, 751.
(14) Crawford, M. K.; Corbin, D. R.; Smalley, R. J. In *Amazing Light: A Festschrift in Honor of Charles Hard Townes on His 80th Birthday*; Chaio, R. Y., Ed.; Springer-Verlag: New York, 1996; Vol. 153.
(15) Crawford, M. K.; Dobbs, K. D.; Smalley, R. J.; Corbin, D. R.; Maliszewskyj, N.; Udovic, T. J.; Cavanagh, R. R.; Rush, J. J.; Grey, C. P. *J. Phys. Chem. B* **1999**, *103*, 431.
(16) Jaramillo, E.; Auerbach, S. M. *J. Phys. Chem. B* **1999**, *103*, 9589.
(17) Böhm, H. J.; Ahlrichs, R.; Scharf, P.; Schiffer, H. *J. Chem. Phys.* **1984**, *81*, 1389.
(18) Böhm, H. J.; Meissner, C.; Ahlrichs, R. *Mol. Phys.* **1984**, *53*, 651.
(19) Gough, C. A.; DeBolt, S. E.; Kollman, P. A. *J. Comput. Chem.* **1992**, *13*, 963.
(20) Vega, C.; Saager, B.; Fischer, J. *Mol. Phys.* **1989**, *68*, 1079.
(21) Lísal, M.; Budinský, R.; Vacek, V.; Aim, K. *Int. J. Thermophys.* **1999**, *20*, 163.
(22) Yamamoto, R.; Kitao, O.; Nakanishi, K. *Fluid Phase Equilib.* **1995**, *104*, 349.
(23) Lísal, M.; Vacek, V. *Fluid Phase Equilib.* **1996**, *118*, 61.
(24) Lísal, M.; Vacek, V. *Mol. Phys.* **1996**, *87*, 167.
(25) Lísal, M.; Vacek, V. *Fluid Phase Equilib.* **1997**, *127*, 83.
(26) Higashi, S.; Takada, A. *Mol. Phys.* **1997**, *92*, 641.
(27) Heublein, G.; Kühmstedt, R.; Kadura, P.; Dawczynski, H. *Tetrahedron* **1970**, *26*, 81.
(28) Fermeglia, M.; Pricl, S. *Fluid Phase Equilib.* **1999**, *166*, 21.
(29) Papasavva, S.; Illinger, K. H.; Kenny, J. E. *J. Phys. Chem.* **1996**, *100*, 10100.
(30) Martell, J. M.; Boyd, R. J. *J. Phys. Chem.* **1992**, *96*, 6287.
(31) Martell, J. M.; Boyd, R. J.; Shi, Z. *J. Phys. Chem.* **1993**, *97*, 7208.
(32) Chen, Y.; Paddison, S. J.; Tschuikow-Roux, E. *J. Phys. Chem.* **1994**, *98*, 1100.
(33) George, A. R.; Freeman, C. M.; Catlow, C. R. A. *Zeolites* **1996**, *17*, 466.
(34) Mellot, C. F.; Cheetham, A. K. *J. Phys. Chem. B* **1999**, *103*, 3864.
(35) Lim, K. H.; Jousse, F.; Auerbach, S. M.; Grey, C. P. *J. Phys. Chem. B* submitted.
(36) Discover 2.9.7/95.0/3.0.0 user guide; Biosym/MSI: San Diego, CA, 1995.
(37) Mellot, C. F.; Davidson, A. M.; Eckert, J.; Cheetham, A. K. *J. Phys. Chem. B* **1998**, *102*, 2530.
(38) Mellot, C. F.; Cheetham, A. K.; Savitz, S.; Gorte, R. J.; Myers, A. L. *J. Am. Chem. Soc.* **1998**, *120*, 5788.
(39) Mellot, C. F.; Cheetham, A. K.; Harms, S.; Savitz, S.; Gorte, R. J.; Myers, A. L. *Langmuir* **1998**, *14*, 6728.
(40) Schrimpf, G.; Schlenkrich, M.; Brickmann, J.; Bopp, P. *J. Phys. Chem.* **1992**, *96*, 7404.
(41) Engelhardt, G. *Microporous Mater.* **1997**, *12*, 369.
(42) Ciraolo, M. F.; Norby, P.; Hanson, J. C.; Corbin, D. R.; Grey, C. P. *J. Phys. Chem. B* **1999**, *103*, 346.
(43) Knözinger, H.; Huber, S. *J. Chem. Soc., Faraday Trans.* **1998**, *94*, 2047.
(44) Löwenstein, M. *Am. Mineral.* **1954**, *39*, 92.
(45) Davis, D. W.; Banna, M. S.; Shirley, D. A. *J. Chem. Phys.* **1974**, *60*, 237.
(46) Meyer, C. W.; Morrison, G. *J. Phys. Chem.* **1991**, *95*, 3860.
(47) Ogata, T.; Miki, Y. *J. Mol. Struct.* **1986**, *140*, 49.
(48) Mukhtarov, I. A.; Kuliev, V. A. *Izv. Akad. Nauk Az. SSR, Ser. Fiz.-Tekh. Mat. Nauk* **1970**, *1–2*, 132.
(49) Brown, D. E.; Beagley, B. *J. Mol. Struct.* **1977**, *38*, 167.
(50) Klaboe, P.; Nielsen, J. R. *J. Chem. Phys.* **1960**, *32*, 899.
(51) Cavalli, L.; Abraham, R. J. *Mol. Phys.* **1970**, *19*, 265.
(52) Kalasinsky, V. F.; Anjaria, H. V.; Little, T. S. *J. Phys. Chem.* **1982**, *86*, 1351.
(53) Brier, P. N. *J. Mol. Struct.* **1970**, *6*, 23.
(54) Danti, A.; Wood, J. L. *J. Chem. Phys.* **1959**, *30*, 582.
(55) Lopata, A. D.; Durig, J. R. *J. Raman Spectrosc.* **1977**, *6*, 61.
(56) Weiner, S. J.; Kollman, P. A.; Nguyen, D. T.; Case, D. A. *J. Comput. Chem.* **1986**, *7*, 230.
(57) Halgren, T. A. *J. Am. Chem. Soc.* **1992**, *114*, 7827.
(58) Gao, G. T.; Wang, W.; Zeng, X. C. *Fluid Phase Equilib.* **1999**, *158–160*, 69.
(59) Catlow, C. R. A.; Freeman, C. M.; Vessal, B.; Tomlinson, S. M.; Leslie, M. *J. Chem. Soc., Faraday Trans.* **1991**, *87*, 1947.
(60) Auerbach, S. M.; Henson, N. J.; Cheetham, A. K.; Metiu, H. I. *J. Phys. Chem.* **1995**, *99*, 10600.
(61) Kirkpatrick, S.; Gelatt, C. D.; Vecchi, M. P. *Science* **1983**, *220*, 671.
(62) Henson, N. J. Ph.D. Thesis, Oxford University, 1996.
(63) Fitch, A. N.; Jobic, H.; Renouprez, A. *J. Phys. Chem.* **1986**, *90*, 1311.

Cation Migration in Dry Zeolites

J. Phys. Chem. B, Vol. 105, No. 49, 2001 **12329**

(64) Allen, M. F.; Tildesley, D. J. *Computer Simulation of Liquids;* Oxford Science Publications: Oxford, U.K., 1987.

(65) Snyman, J. A. *Comput. Math. Appl.* **1989**, *17*, 1369.

(66) Eulemberger, G. R.; Shoemaker, D. P.; Keil, J. G. *J. Phys. Chem.* **1967**, *71*, 1812.

(67) Vitale, G.; Mellot, C. F.; Bull, L. M.; Cheetham, A. K. *J. Phys. Chem. B* **1997**, *101*, 4559.

(68) Auerbach, S. M.; Bull, L. M.; Henson, N. J.; Metiu, H. I.; Cheetham, A. K. *J. Phys. Chem.* **1996**, *100*, 5923.

(69) Mortier, W. J. *Compilation of Extraframework Sites in Zeolites*; Butterworth-Heinemann: London, 1982.

(70) Olson, D. H. *Zeolites* **1995**, *15*, 439.

(71) Nosé, S. *J. Chem. Phys.* **1984**, *81*, 511.

(72) Hoover, W. G. *Phys. Rev. A* **1985**, *31*, 1695.

(73) Martyna, G. J.; Klei, M. L.; Tuckerman, M. E. *J. Chem. Phys.* **1992**, *97*, 2635.

(74) Jang, S.; Voth, G. A. *J. Chem. Phys.* **1997**, *107*, 9514.

(75) Tuckerman, M. E.; Martyna, G. J. *J. Chem. Phys.* **1999**, *110*, 3623.

(76) Jang, S.; Voth, G. A. *J. Chem. Phys.* **1999**, *110*, 3626.

(77) Tuckerman, M. E.; Martyna, G. J. *J. Chem. Phys.* **1999**, *111*, 3313.

(78) Berens, P. H.; Wilson, K. R. *J. Chem. Phys.* **1981**, *74*, 4872.

(79) Grey, C. P.; Ciraolo, M. F.; Lim, K. H. In *Proceedings of the 12th International Zeolite Conference*; Treacy, M. M. J., Marcus, B. K., Bisher, M. E., Higgins, J. B., Eds.; Materials Research Society: Warrendale, PA, 1999.

(80) Myers, A. L. Personal communication.

(81) Savitz, S.; Siperstein, F. R.; Huber, R.; Tieri, S. M.; Gorte, R. J.; Myers, A. L.; Grey, C. P.; Corbin, D. R. *J. Phys. Chem. B* **1999**, *103*, 8283.

(82) Lievens, J. L.; Mortier, W. J.; Chao, K. J. *J. Phys. Chem. Solids* **1992**, *53*, 1163.

(83) Pimentel, G. C.; McClellan, A. L. *The Hydrogen Bond;* W. H. Freeman: San Francisco, CA, 1960.

(84) Baker, M. D.; Godber, J.; Ozin, G. A. *J. Am. Chem. Soc.* **1985**, *107*, 3033.

(85) Godber, J.; Baker, M. D.; Ozin, G. A. *J. Phys. Chem.* **1989**, *93*, 1409.

(86) Rodriguez, A. *Vib. Spectrosc.* **1995**, *9*, 225.

(87) Olliff, M. P.; Fischer, G. *Spectrochim. Acta* **1994**, *50A*, 2223.

(88) McNaughton, D.; Evans, C.; Robertson, E. G. *J. Chem. Soc., Faraday Trans.* **1995**, *91*, 1723.

(89) Newnham, D.; Ballard, J.; Page, M. *J. Quant. Spectrosc. Radiat. Transfer* **1996**, *55*, 373.

(90) Xu, L. H.; Andrews, A. M.; Cavanagh, R. R.; Fraser, G. T.; Irikura, K. K.; Lovas, F. J.; Grabow, J. U.; Stahl, W.; Crawford, M. K.; Smalley, R. J. *J. Phys. Chem. A* **1997**, *101*, 2288.

(91) Beukes, J. A.; Nicolaisen, F. M. *J. Quant. Spectrosc. Radiat. Transfer* **2000**, *66*, 185.

(92) Smith, K.; Newnham, D.; Page, M.; Ballard, J.; Duxbury, G. *J. Quant. Spectrosc. Radiat. Transfer* **1998**, *59*, 437.

(93) Voter, A. F. *J. Chem. Phys.* **1997**, *106*, 4665.

(94) Voter, A. F. *Phys. Rev. Lett.* **1997**, *78*, 3908.

(95) Dellago, C.; Bolhuis, P. G.; Csajka, F. S.; Chandler, D. *J. Chem. Phys.* **1998**, *108*, 1964.

(96) Dellago, C.; Bolhuis, P. G.; Chandler, D. *J. Chem. Phys.* **1998**, *108*, 9236.

(97) Dellago, C.; Bolhuis, P. G.; Chandler, D. *J. Chem. Phys.* **1999**, *110*, 6617.